Journal of Water Process Engineering 41 (2021) 102011

Contents lists available at ScienceDirect

Journal of Water Process Engineering

journal homepage: www.elsevier.com/locate/jwpe

Data fusion to monitor remineralisation of desalinated groundwater in calcite contactors

Dirk Vries [a,*], Martin Korevaar [a], Sara Ghanbari [b], Gerard van Houwelingen [c], Walter van der Meer [b,d]

[a] KWR Water Research Institute, Nieuwegein, the Netherlands
[b] Oasen N.V., Gouda, the Netherlands
[c] Royal HaskoningDHV, Amersfoort, the Netherlands
[d] University of Twente, Enschede, the Netherlands

ARTICLE INFO

Keywords:
Calcite filtration
Model
Software sensor
Water treatment
Remineralisation

ABSTRACT

The emergence of organic micropollutants in surface waters and even groundwater and increasing salination in river delta areas, drives water utility managers towards adoption and application of advanced and robust barriers in drinking water production like reverse osmosis (RO) filtration. However, water produced by RO, called permeate, contains hardly any minerals, is corrosive and bitter in taste. Hence, remineralisation is needed to improve the permeate water quality and comply with (Dutch) drinking water regulation. In order to test the performance of remineralisation using limestone (calcite) filtration, a pilot-scale filter has been set up and connected to an RO filtration system that treats anaerobic groundwater and equipped with on-line sensors for pH, conductivity and carbon dioxide. The degree of (re)mineralisation was tested at different flow rates, a smaller calcite grain size and with a lower temperature than previous studies. The pilot shows that the degree of remineralisation performance can be monitored on the basis of a few on-line sensors and a model that describes the dissolution of calcite.

1. Introduction

Limestone filtration, also called marble filtration or more specifically, calcite filtration, is a widely used, and relatively inexpensive technique to condition soft, desalinated water to a desired water hardness and alkalinity such that the filtered water is suited for potable use [1]. To this end, a contactor is filled with calcite (i.e. calcium carbonate) granules and (permeate) water is filtrated through. Besides temperature, the rate of dissolution of calcite is determined by raw water chemistry, i.e. pH, alkalinity and lime carbonic equilibrium reactions, and on physical aspects such as the filtration rate and contact time. Despite the availability of literature on the subject of calcite dissolution rate and the accumulation of a large data set over the past four decades (see the review papers of [2–4]), there is significant uncertainty in the absolute value of the dissolution rate under given conditions [5].

In the Netherlands, the production and supply of drinking water should comply with the Dutch Drinking Water Directive [6]. The directive states that drinking water should contain a hardness (i.e. Calcium and Magnesium concentration) of at least 1 mmol per liter and 60 mg per liter bicarbonate as a minimum concentration. Hence, a method to design and operate calcite contactors for the purpose of drinking water production or, more generally, conditioning of desalinated water, is relevant to ensure optimal operation and reduce costs related to finding an optimal design. Costs for calcite dissolution are estimated at 0.05 to 0.10 $/m^3 [7]. The combination of reverse osmosis (RO) and post-treatment by the application of calcite contactors could be an economic feasible approach for the production of potable water for regions where there is brackish groundwater as e.g. in the Mediterranean countries or the Middle East region [8,9], fluoride contaminated [10] or micro-pollutant contaminated groundwater, river bank filtrate [11] or surface water [12]. For example, RO followed by remineralisation is going to be implemented at full-scale to treat riverbank filtrate for potable water production at an actual treatment plant located in the Dutch municipality of Woerden [13].

To the aim of contactor design, calcite dissolution models have been developed in the eighties and nineties [14,15] and have been discussed and successfully adopted for desalination applications in recent years [16,17]. In these papers, and as far as we know, (i) the dissolution rate is

* Corresponding author.
E-mail address: dirk.vries@kwrwater.nl (D. Vries).

https://doi.org/10.1016/j.jwpe.2021.102011
Received 16 June 2020; Received in revised form 2 February 2021; Accepted 4 March 2021
Available online 23 March 2021

not described unambiguously for low (groundwater) temperatures and relatively small calcite granule sizes (<1 mm), and (ii), the (simplified) contactor calcite dissolution model has not been used to support daily operation. In this paper, we adopt the model as described in [14] and [15] and evaluate its sensitivity regarding different parameters, including granule size. Furthermore, we assess its benefits and limitations when fusing this model with data from a calcite contactor on pilot scale applied to desalinated, low temperature groundwater.

2. Methods

2.1. Pilot scale experiments

2.1.1. Setup

A stainless steel contactor (fabricated by Logisticon) in cylindrical form with radius 0.318 mm and bed height 2.5 m and 20 manually operated sampling points is connected to a buffer tank that holds RO permeate of treated bank filtrate water, see Fig. 1 for a schematic overview. The permeate stream, contactor influent and filtrate stream are monitored by pH sensors (AMI-2, Swan analytical instruments) and electrical conductivity (EC) (Powercon Specific EC, AMI-2, Swan analytical instruments). CO_2 is measured in the influent stream of the contactor (CGP-31 Turbitrack, DKK-DOA). The contactor was filled with either calcite grains having a size ranging from 0.5 to 1.2 mm or 1–2 mm, an apparent density of 2700 kg/m3 and initial bulk density of 1340 kg/m3. Via a volumetric method, the intra-particulate porosity was calculated and reads a value of 0.53.

2.2. Influent water of calcite contactor

The pilot scale calcite contactor was fed with groundwater treated by reverse osmosis (RO) membrane filtration. This water has had post-treatment by ion exchange to remove the remaining ammonium. Table 1 below lists the average permeate water quality during the experimentation period.

2.3. Model and data fusion approach

2.3.1. Steady state equilibrium model

The calcite dissolution reaction is described by the uptake of carbon dioxide and water molecules such that calcium and bicarbonate are released.

$$CaCO_3 + CO_2 + H_2O \rightarrow Ca^{2+} + 2HCO_3^- \quad (1)$$

The reaction is governed by two equilibrium reactions, i.e. the equilibrium of carbon dioxide with water and a bicarbonate

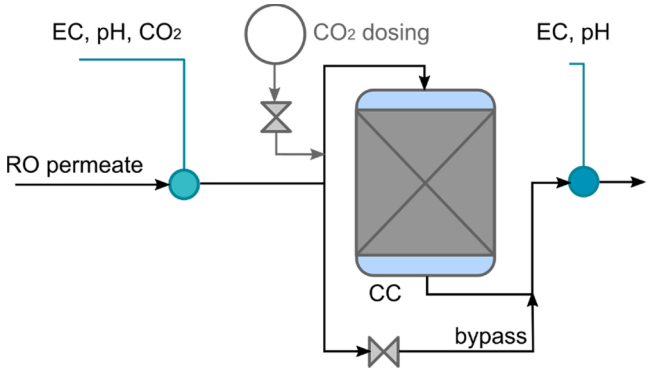

Fig. 1. Schematic overview of the calcite contactor pilot setup. The influent of the calcite contactor (CC) is equipped with EC, pH and CO_2 sensors (sea-green) and the effluent side with an EC and pH sensor. A carbon dioxide dosing point precedes the calcite contactor and the flow of the bypass permeate stream is controlled by a valve.

Table 1
Average or minimum and maximum value of the water quality characteristics of the feed water (LLOD: lower limit of detection reached).

Parameter	Unit	Value
Chloride	mg/L Cl	1.3; 2.0
Sodium	mg/L Na	3.5; 4.0
Sulphate	mg/L SO_4	0.20 (LLOD)
Bicarbonate	mg/L HCO_3	7.9; 12.0
pH	–	5.2; 5.7
CO_2	mg/L CO_2	45; 85
Calcium*	mg/L Ca	0.01; 0.07
Iron*	mg/L Fe	≤ 0.01 (LLOD)
Magnesium*	mg/L Mg	≤ 0.1 (LLOD)
Methane	mg/L CH_4	1.3; 2.5
Temperature	°C	10.0; 12.0
EC	µs/cm	15; 24

* As the feed water is RO permeate, bivalent and trivalent ions are not present or fall below the detection limit.

equilibrium. The corresponding equilibrium constants K_1 and K_2 are written from

$$\{CO_2\} + \{H_2O\} \leftrightarrow^{K_1} \{HCO_3^-\} + \{H^+\} \quad (2)$$

$$\{HCO_3^-\} \leftrightarrow^{K_2} \{CO_3^{2-}\} + \{H^+\} \quad (3)$$

Finally, solubility is governed by the activities of calcium and carbonate ions

$$CaCO_3 \leftrightarrow^{K_{sp}} \{Ca^{2+}\} + \{CO_3^{2-}\} \quad (4)$$

$$\{x\} = \gamma_x[x] \quad (5)$$

By combining Eqs. (1)–(4) a relation can be found when a solution having an (initial) concentration of CO_2 is brought in contact with a surplus of calcite. This leads to an equilibrium where the CO_2 concentration reads:

$$\{CO_2\}_e = \frac{K_2}{2K_1K_{sp}}\left(\{HCO_3^-\}_e^3\right); \quad (6)$$

here the subscript e refers to the equilibrium concentrations. Furthermore, Eq. (1) describes that for 1 mol of dissolved Ca^{2+}, 1 mol of CO_2 disappears while 2 mol of HCO_3^- is formed. Thus,

$$\begin{aligned}[CO_2]_e &= [HCO_3^+]_{init} + [CO_2]_{init} - 2[HCO_3^-]_e \\ &= [Ca^{2+}]_{init} + [CO_2]_{init} - [Ca^{2+}]_e. \end{aligned} \quad (7)$$

With the subscipt init referring to the initial concentration. When dealing with non-ideal solutions, (8) is written in activities instead of concentrations i.e. $\{x\} = \gamma_x[x]$ can be substituted in (7). This leads to an expression of the equilibrium CO_2 concentration for a given initial CO_2 concentration (see e.g. [16]). However, the acquired results are not always accurate as one has to include the effect of the change of pH during the dissolution of $CaCO_3$ and changes in solubility due to charge and electrical double layer effects on the surface of calcite.

2.3.2. Calculating the dissolution trajectory

Assuming that equilibrium will be fully reached, one can calculate the required dose of aggressive CO_2 in the influent by the aid of (6) and the ratio of (required) formation of HCO_3^- with respect to the amount of CO_2 that is required in a closed system. Graphically one can visualise the calcite dissolution trajectory as the line connecting the initial CO_2 (vertical axis) and bicarbonate concentration (horizontal axis) point with the intersection point of the solubility Eq. (6) at the desired bicarbonate concentration - see Fig. 2. In other words, initially, water contains a given amount of CO_2 (and no, or very little HCO_3^- and Ca^{+2}) and is brought into contact with calcite. As soon as water gets into contact with calcite, the dissolved CO_2 reacts, resulting in a decrease of CO_2 concentration and an increase in HCO_3^- concentration (walking

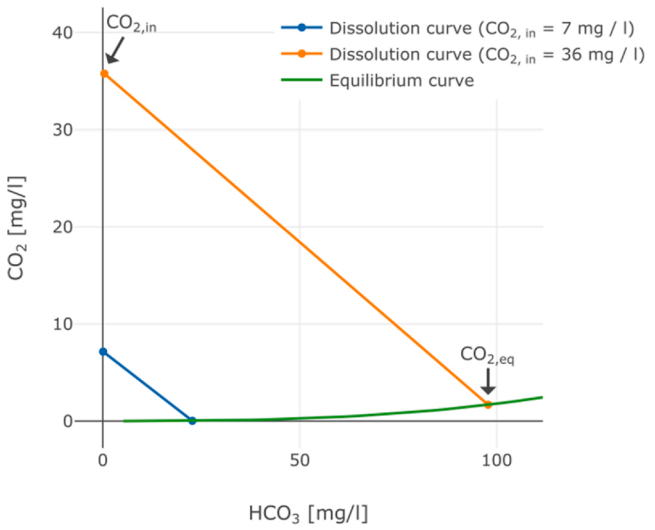

Fig. 2. CO_2 and HCO3- concentrations for water that is brought in contact with a surplus of calcite. The green line indicates the equilibrium concentration ratios Eq. (7); the blue and orange line indicate the change in ratio of water that starts with very little HCO_3^- and 7 respectively 36 mg/l CO_2 in solution; for the orange line this is indicated by CO_2,in. As the water reacts with calcite, CO2 concentration decreases while HCO_3^- concentration increases; the orange and blue line have a negative slope. This continues until it reaches the equilibrium concentration (indicated by CO_2,eq) ratio given by the green line. Note how the dissolution curves are straight lines as given by Eq. (1).

from the left point in e.g. the orange or blue line in Fig. 2 to the right). When there is an abundant amount of $CaCO_3$ present, this process continues until the equilibrium concentrations are reached (i.e. the orange or blue line intersects the green solubility line).

In a calcite contactor, this same process happens, albeit under the condition that the residence time is too short to achieve complete equilibrium. Two mechanism can be identified that limit the dissolution: (1) the kinetics of the dissolution itself as described by [2] and (2) the (diffusive) mass transfer of the Ca^{2+}, HCO_3^- and CO_2 molecules through the diffuse film layer around the calcite particles [14,15]; the models from these two papers are hereafter referred to as Yamauchi model [15] and Letterman model [14] respectively. When one of the limiting mechanisms is much slower than the other, the fastest mechanism can be ignored because the slowest determines the rate. Because calcite contactors are generally applied as packed bed reactors, mass transfer is likely to be the limiting mechanism. Indeed, [7,15–17] showed that the Yamauchi model, that assumes infinitely fast dissolution kinetics, predicted the concentration of Ca^{2+}, HCO_3^- and CO_2 correctly over the whole bed height for different velocities. Because the Letterman and Yamauchi model have shown to be reliable models for calcite contactors these models are applied in this work as well; they are described in the following section.

Both the Yamauchi model and the Letterman model assume mass transfer in a packed bed with plug flow. For one component, say A, in the solution, this can be described with dispersed plug-flow model:

$$N_{D,A}\frac{d^2C_A}{dZ^2} - \varepsilon\frac{dC_A}{dZ} + r_A\bar{t} = 0. \tag{8}$$

Here, the subscript denotes the quantity belongs to the component A; N_D is the dimensionless axial dispersion number; C the concentration (in the bulk of the fluid); Z the dimensionless axial distance ($Z = z/L$); L is the height of the reactor; ε the porosity of the bed; r the overall dissolution reaction rate; and $\bar{t} = \frac{u}{L}$ the residence time of the reactor; and u the superficial velocity of the fluid. In this system, the reaction rate describes how fast the compound A is entering the bulk fluid.

In a developed flow, the following relation holds for mass transfer through a film layer

$$r = k_A\, a\left(C_{A,s} - C_A\right) \tag{9}$$

where k overall dissolution rate constant per surface area of grain; a is the interfacial area of the grain's surface per volume of liquid; and $C_{A,s}$ the concentration of A at the grain's surface which equals $C_{A,eq}$ under the assumption that dissolution is much faster than film layer transport. With the particle diameter d and its sphericity Ψ, a can be written as

$$a = \frac{6(1-\varepsilon)}{d\,\varepsilon\,\Psi}. \tag{10}$$

After substitution of (9) and (10) in (8), neglecting axial dispersion and integrating the results yields:

$$\ln\left(\frac{C_A(z) - C_{A,eq}}{\left(C_A(z=0) - C_{A,eq}\right)}\right) = -k_A\frac{6(1-\varepsilon)}{d\,\Psi}\frac{z}{u} \tag{11}$$

Or, with $k^{'} = 6k_A/\Phi$ and rewriting Eq. (11):

$$C_A(z) = \left(C_A(z=0) - C_{A,eq}\right)e^{-k^{'}\frac{(1-\varepsilon)}{d}\frac{z}{u}} + C_{A,eq}. \tag{12}$$

In [14] C_A is substituted by Ca^{2+}, in [15] it is substituted by CO_2. Eq. (12) is used in this work to model the calcite dissolution of the reactor, and $6k_A/\Psi$ is determined empirically.

2.3.3. Kinetic dissolution constant

In [14], the contribution of dissolution kinetics, diffusion through the liquid film layer and diffusion through the calcite grain's pores is taken into account with distinct model equations. These equations are supplied with physics to be able to theoretically determine the value of k_A ; for example, relations that describe the boundary layer thickness (and thus the mass transfer rate) as function of the superficial velocity. This is appealing because it allows for a prediction of reactor performance based on reactor configuration, water composition and calcite properties alone. However, despite the increased complexity these equations cannot predict k_A accurately and one has to rely on empirical relations. The suggested reason for this is that surface interactions are important but cannot be captured in a model (yet) [7,17,18].

Table 2 compiles a list of kinetic dissolution constants under various temperature, (empty bed) contact times and calcite grains. The value of k' is reported to be related to the square root of the filtration velocity [17]. However their proposed relationship relies on 3 data points only. Moreover, the filtration velocity does not appear to have a significant contribution for the collected values of k' (Table 2) in case other factors could play a role - see Fig. 3. It is important to note that differences of these k' values may also be attributed to differences in operating temperatures and calcite material characteristics. For example, [17] report that in practice, the quotient $6k_A/\Phi$ can differ up to 70 % due to differences in morphology and size distribution of calcite grains, while process conditions, average grain size and calcite content do not differ significantly. We assessed whether other parameters could explain the differences in k'. Temperature is a likely candidate and is reported to indeed have an influence [19]. Data of all literature sources as cited in Table 2, show that the influence of temperature on k' is significant and indicates a relation with activation energy E_a according to the well-known Arrhenius relation $k' \sim \exp(-E_a/(RT))$, see Fig. 4.

2.3.4. Data fusion approaches

Different measuring options exist to allow monitoring of filtrate water quality, and more specifically, allow feedforward control of calcite contactors. We list the following options:

- measure CO_2 and measure pH (and temperature) in the permeate stream, than calculate the initial HCO_3^- concentration;

Table 2
Overview of dissolution constants found in literature as well as the conditions under which they are determined.

Type of limestone	Bed height m	Influent water Temperature Celsius	Bed porosity [-]	Average grain size mm	Superficial velocity m/h	6k/Phi ($\cdot 10^6$) m/s	Source
Aqua-juraperle TWA	2	12	0.5	0.85	10	4.9	[18]
					16.5	6.3	[18]
					28.7	8.3	[18]
			0.49	1.5	10	4.8	[18]
					16.5	6.1	[18]
					28.7	8.2	[18]
A (Zmitut 81)	1.8	28.6	0.44	2	9.4	10.5	[17]
A (Zmitut 81)		22	0.44	2	9.9	6.95	[19]
A (Zmitut 81)					16.4	7.13	[19]
A (Zmitut 81)					27.3	7.31	[19]
A (Zmitut 81)		30	0.44	2	16.4	12	[19]
Akdolit	1.8	30	0.38	2.85	14.8	25	[16]
Not reported		40	0.42	5.7	20	28	[15]
Not reported	Not reported	22.4	Not reported	3	10	7.19	[21]
					20	11.3	[21]
					30	11.6	[21]

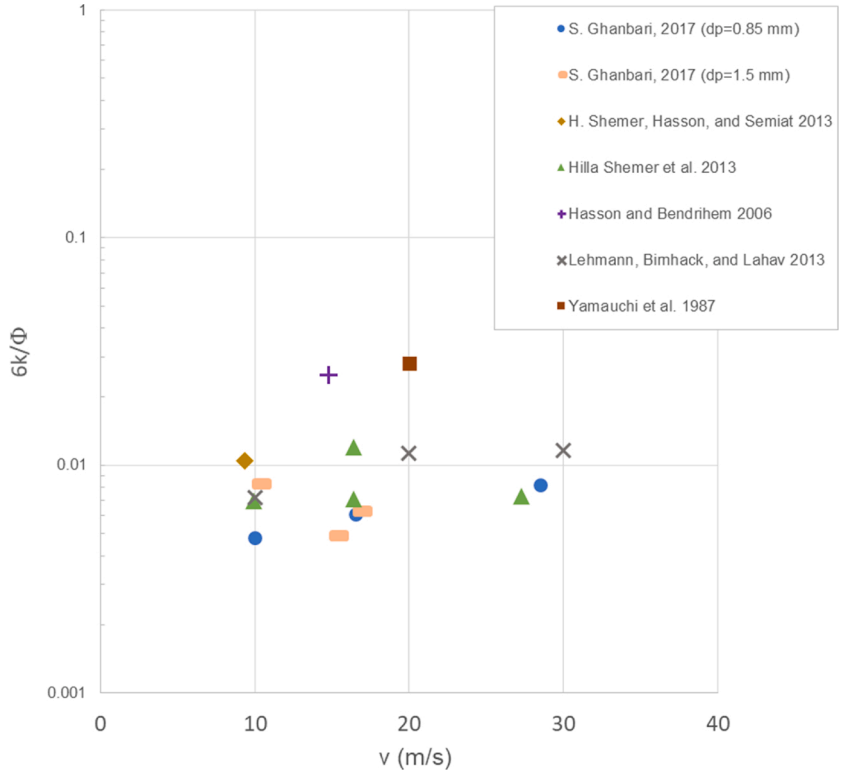

Fig. 3. Variation of the quotient 6k/Φ for various filtration velocities on a logarithmic scale. Values are based on Table 1.

- obtain the HCO_3^- concentration by using a permeate stream EC calibration standard and measure pH (and temperature) in the permeate stream, than calculate the initial CO_2 concentration;
- obtain the HCO_3^- concentration by using a permeate stream EC calibration standard and measure CO_2 (and temperature) in the permeate stream, than calculate the pH of the permeate;
- measure (upstream) the pH of the membrane feed and measure CO_2 at the permeate stream, or obtain the HCO_3^- concentration by using a permeate stream EC calibration standard. Than either calculate the bicarbonate concentration or the CO_2 concentration depending on the use case.

Subsequently, the triplets of two measured and one calculated value (*), i.e. $\{[CO_2], pH, [HCO_3^-]^*\}^{(1)}$, $\{[CO_2]^*, pH, [HCO_3^-]\}^{(2)}$ and $\{[CO_2], pH^*, [HCO_3^-]\}^{(3)}$ for case (1), (2), and (3) respectively, allow for calculating the equilibrium concentration and hence solving Eq. (12) near real time provided measurements are recorded (near) real time.

The accuracy and reliability of approaches (1) to (3) will be assessed in the results section, approach 4 fell outside the scope of this study.

2.3.5. Model simulations

The filtrate water quality was simulated based on the (on-line) measurement data of the permeate, contactor dimensions, calcite material characteristics and process conditions. The model was run on an Intel i3 powered laptop using Python for data processing, calcite kinetics and visualisation and Phreeqc [20] for calculating the speciation of calcite dissolution and account for the change of pH during the dissolution of $CaCO_3$ and charge effects on the surface of calcite.

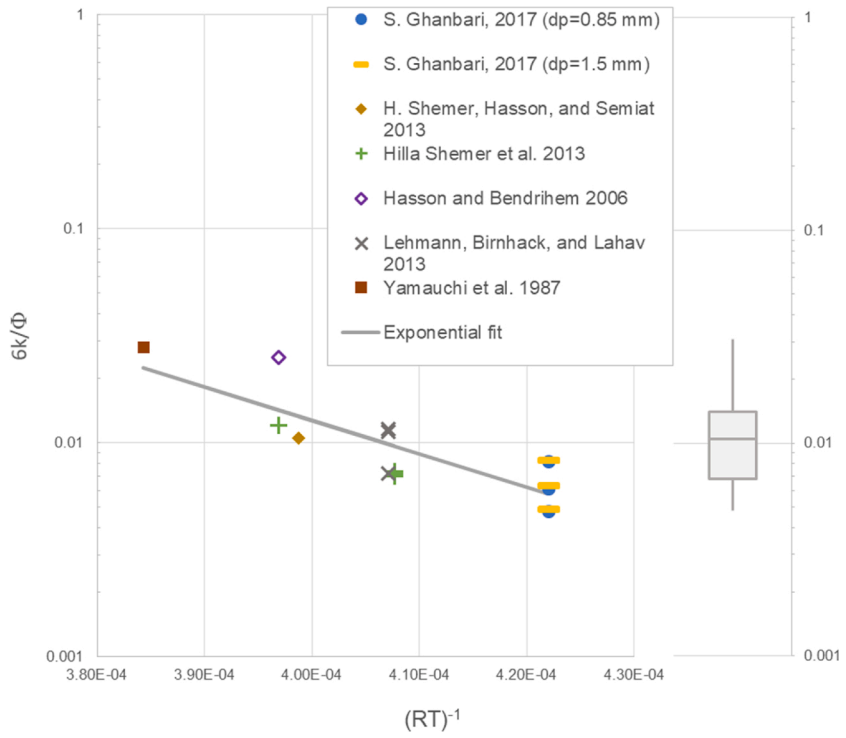

Fig. 4. The quotient 6k/Φ plotted against temperature on a logarithmic scale.

3. Results and discussion

3.1. Parameter sensitivity analysis

3.1.1. Modelled conversion efficiency

In order to assess the importance of parameters that drive the conversion of the dissolution of CO_2 (or Ca^{2+}), the conversion ratio is defined [15]:

$$\eta = \frac{C_A(z=0) - C_A(z)}{C_A(z=0) - C_{A,eq}} \tag{13}$$

Using Eq. (13) and with the calibrated value of k_A using pilot scale data [18], the efficiency of conversion is compared with results found in literature (Fig. 5). The figure shows that the pilot experiment conditions and (relatively speaking) fine grain material in [18] with a grain diameter of 1.0–2.0 mm lead to approximately the same conversion efficiency as reported by [15] and hence counteract the operating temperature of 40 degrees Celsius and coarse grain material (5.7 mm) as reported in their work. A larger grain size generally lead to lower efficiency as shown by the purple line with diamond shaped markers, while higher temperatures lead to higher efficiencies [17] compared to the reference data [18].

In addition to the theoretical conversion ratio (or efficiency) as in Eq. (13), we write the apparent conversion (or, here also referred to as the dissolution efficiency) as the difference of inlet concentration compared to the outlet concentration relative to the inlet concentration:

$$\eta_{app} = \frac{C_A(z=0) - C_A(z)}{C_A(z=0)} \tag{14}$$

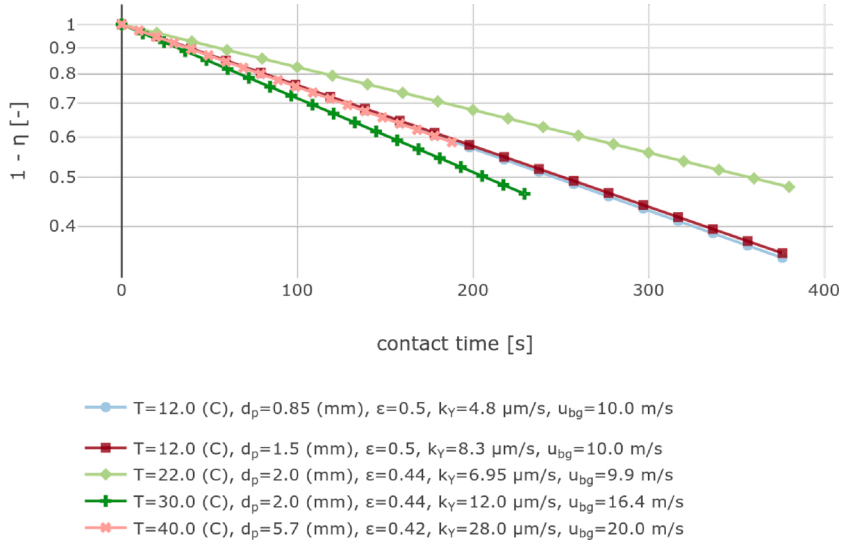

Fig. 5. Comparison of efficiencies in conversion compiled from literature for various process conditions and calcite grains ([18]: •, ■; [15]: x; [17]: +, ♦).

The grain size and height of the calcite bed are typical design parameters to steer the calcite dissolution process without affecting the influent water quality. Figs. 6 and 7 show the apparent and theoretical conversion efficiency of calcite, or similarly carbon dioxide, for varying grain sizes (left pane) and filter bed heights (right pane of both figures). Note that the effect of the filter bed height can be traced back to the change in filtration velocity to keep the contact time the same for different filter bed heights. Furthermore, the theoretical conversion efficiency will always be larger than the apparent conversion, due to the equilibrium concentration being larger than zero. Conversely, one minus the theoretical conversion will be smaller than for the apparent conversion case. Indeed, a smaller grain size and higher filtration velocity promote calcite dissolution. Clearly, Eq. (12) dictates that both the grain size as well as the filter bed height (or filtration velocity) have a significant effect, but their effects become less pronounced with increasing residence time.

In addition, we investigated the effect of grain size and porosity as well as the influence of the dispersion constant N_D and (imposed) values of the dissolution rate constant k_Y for ground water temperature by plotting the efficiency of conversion against empty bed contact time, see Figs. 2 and 3 in the Supplementary material.

The dissolution of calcite is heavily dependent on the carbon dioxide equilibrium equations. The effects of pH and CO_2 present in the influent (here: RO permeate stream) on the apparent conversion efficiency is shown in Fig. 8. Here, we see that the apparent (measurable) conversion increases with decreasing pH and decreasing CO_2. At the same pH, less carbon dioxide is dissolved than is the case if the system would be in equilibrium, and hence more bicarbonate will be present in the system. Consequently, the apparent conversion is higher for lower values of CO_2 concentration. Similarly, lower pH leads to a more favourable shift of CO_2 to bicarbonate. The difference for different pH or CO_2 concentrations increases with increasing bed contact time. This makes sense as the driving force does not change with changing residence time, but is altered by the different pH and hence its effect on the equilibrium. The effect of grain size and bed height (Fig. 6) with increasing bed contact time decreases on the apparent conversion: this naturally follows from a convergence analysis of Eq. (12).

Note that the theoretical conversion Eq. (13) does not change with varying values of pH or inlet carbon dioxide concentration (Fig. 4 of the Supplementary materials). The same results are caused by a cancelling out of the change in equilibrium concentration due to change in pH or CO_2 in both the modelling equations Eq. (12) as the equation for the theoretical conversion Eq. (13).

3.1.2. *Effect of pH and initial bicarbonate concentration on CO_2 equilibrium*

The model equations rely heavily on the equilibrium concentration, hence this concentration needs to be determined accurately. Therefore, the CO_2 concentrations of the permeate water need to be known. This can be measured directly or it can be deduced from the pH and HCO_3^- concentrations in the permeate by applying Eqs. (1)–(4) or speciation calculations. Fig. 9 shows the CO_2 equilibrium concentration affected by different water compositions that are brought into contact with an excess amount of calcite. This figure demonstrates the sensitivity of the equilibrium CO_2 concentration to different values of initial pH, and concentrations of HCO_3^- and CO_2. It is clear that if only the HCO_3^- and pH measurements are used, they both need to be accurate. Higher accuracy is required for lower pH or a higher HCO_3^- concentration. Fig. 9 depicts that, at a pH = 4.8, a change or error of 50 % in the HCO_3^- concentration from 6 to 9 mg/L yields an error of 100 % in the equilibrium CO_2 concentration, while at pH = 5.3 the equilibrium concentration drops to less than 20 mg/L CO_2 – i.e. there is more than 50 % less available. Note that a pH of 4.8 corresponds to a 50 % lower H^+ concentration compared to pH value 5, while a pH of 5.3 has a 50 % higher H^+ concentration. Due to the low conductivity of permeate stream, relative large measurement errors are to be expected for both the pH and EC measurements; the EC measurements relate to the HCO_3^- concentration Based on this analysis, we expect that a data fusion approach using the measured values of pH and HCO_3- leads to a (possible) large bias in predicted CO_2 (or HCO_3^-) content in the filtrate of a calcite contactor. On the other hand, less biased is introduced when the combination of pH and CO_2 or CO_2 and HCO_3^- are used. Indeed, this is supported by separate experiments (see Fig. 5 of the Supplementary material and [18]).

On the other hand, the values of pH or HCO_3^- concentrations negligibly influence the equilibrium CO_2 concentration when using CO_2 measurements even if their value is changed by 50 %. In that case, only the CO_2 concentrations need to be accurate (Fig. 10).

3.2. *Data fusion within pilot scale experiments*

The model was fed with different sensor signals to predict the bicarbonate content (such that the theoretical amount of dissolved calcite can be calculated) of the filtrate of a pilot scale calcite contactor. The pilot scale contactor was connected to RO treated infiltrated groundwater, while the groundwater quality was subject to water quality variation due to the well configuration. The well valve configuration changed daily at 8:00 AM. Different data fusion inputs have been tested to predict the bicarbonate concentration in the filtrate ($[HCO_3^-]_f$):

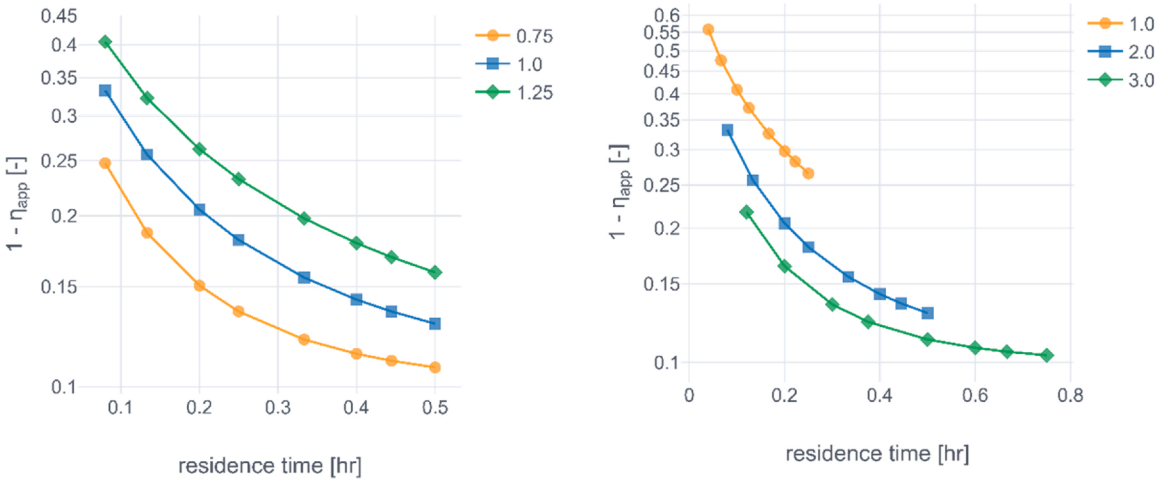

Fig. 6. Influence of the grain diameter in millimetre (see legend, left pane) on the apparent conversion efficiency (left pane) and the influence of the height of the calcite bed (in metre, right pane) on a log scale.

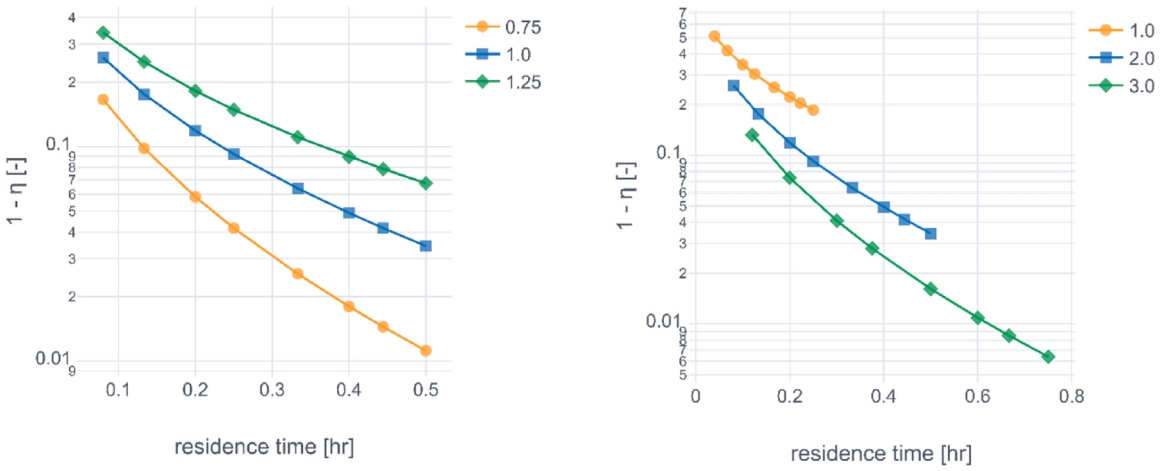

Fig. 7. Influence of the grain diameter in millimetre (see legend) on the theoretical conversion efficiency (left pane) and effect of the filter bed height in metre (see legend) on the conversion efficiency (right pane), both on a log scale.

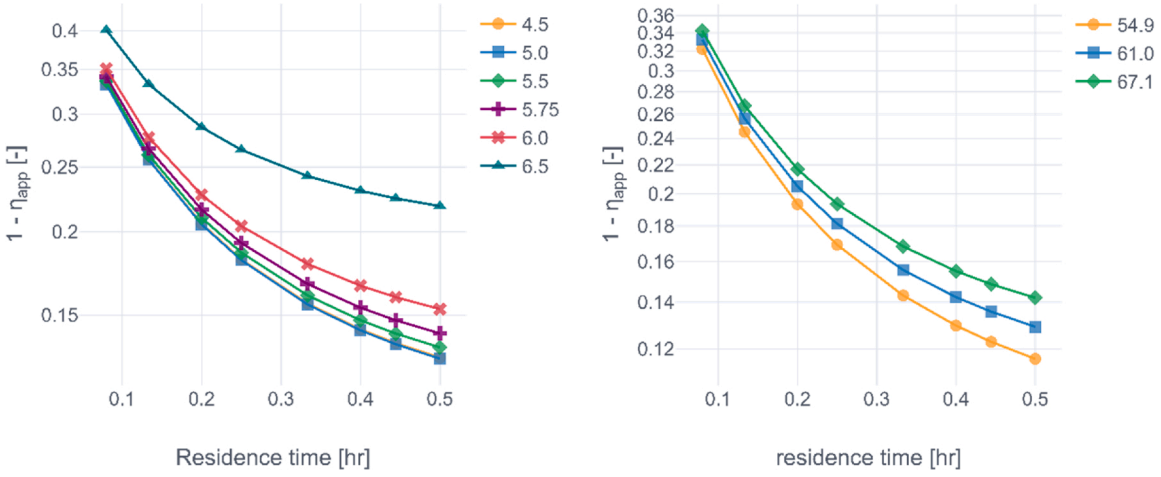

Fig. 8. Influence of the pH value (left pane, see the legend) and the inlet carbon dioxide concentration (in mg/L, right pane) on the apparent conversion efficiency in the influent of a calcite contactor on a log scale.

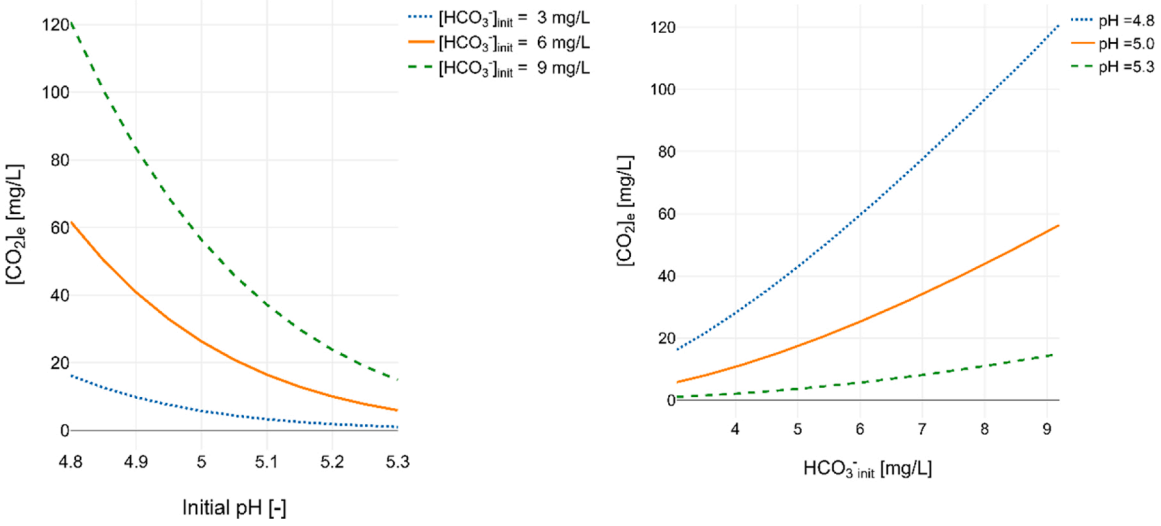

Fig. 9. Simulation results where water with an initial pH and with initial CO_2 concentration is brought into contact with calcite. This yields an equilibrium concentration of CO_2 as indicated by the y-axis. Left pane: initial pH on the horizontal axis, different initial concentrations plotted with different colors. Right pane: same representation as left pane, however, the horizontal axis represent the initial bicarbonate concentration, and different values of pH are represented by different colors.

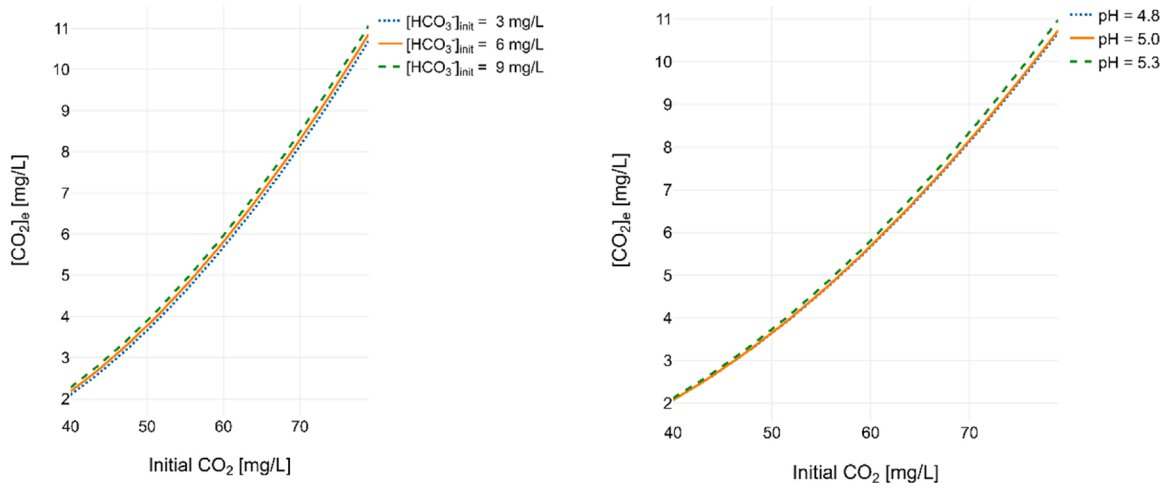

Fig. 10. Same results as in Fig. 9, but now the x-axis indicate the initial CO_2 concentrations; the lines with different colors in the left pane correspond to different HCO_3 – concentrations, and correspond to different initial pH values in the right pane.

- using measurements of CO_2 ($[CO_2]^m$) and HCO_3^- (actually, $[HCO_3^-]^m$ is derived from an EC calibration line – see the Supplementary Material) to predict pH in the permeate (and bicarbonate in the filtrate) i.e. $\{[CO_2]^m, pH, [HCO_3^-]^m\}_p$,
- using $\{[CO_2]^m, pH^m, [HCO_3^-]\}_p$ and
- using $\{[CO_2], pH^m, [HCO_3^-]^m\}_p$.

The predicted $[HCO_3^-]_f$ was compared with calculated $[HCO_3^-]_f$ values via the EC calibration line, results are shown in Fig. 11. Interestingly, noise characteristics are kept reasonably small with the data fusion triplets $\{[CO_2]^m, pH, [HCO_3^-]^m\}$ and $\{[CO_2]^m, pH^m, [HCO_3^-]\}$, while the signal to noise ratio is increased significantly for the triplet $[CO_2], pH^m, [HCO_3^-]^m$. Apparently, the use of a pH sensitive EC measurement in combination with pH measurements lead to multiplication of noise in the model. Clearly, this data duo leads also to a large model bias. The $\{[CO_2]^m, pH^m\}_p$ driven data fusion model slightly overestimates the $[HCO_3^-]_f$ value, but performs much better than (pH^m, $[HCO_3^-]^m$) driven model. From this test run, it seems that the ($[CO_2]^m$, $[HCO_3^-]^m$) driven model performs best of the three. In addition to these data fusion tests, the deviation in CO_2 sensor measurements was assessed with laboratory measurements and EC measurements and the sample standard deviation was estimated as being fairly low with a value of 4.5 %, see the Supplementary material. Note that the (model) bias of the data fusion approaches were minimized by using a slightly smaller value of the grain diameter ($d_p = 1.25$ mm) in the model than would be expected using the size distribution d_{50} value of 1.5 mm. Fig. 12 depicts

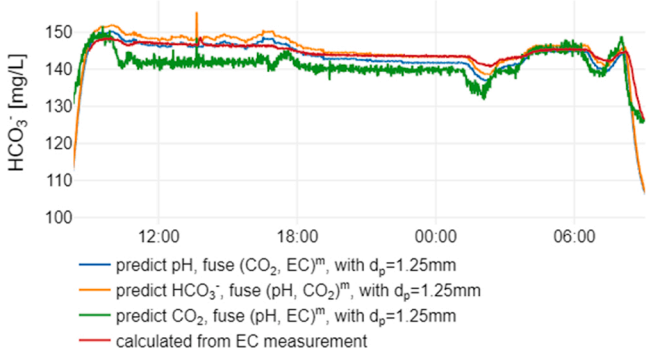

Fig. 11. Predicted bicarbonate concentration at the influent using different data fusion inputs from the influent (blue, orange, green line); the red line indicates bicarbonates concentration based on the measured EC of the effluent. The contactor is operated with a d_{50} of 1.5 mm calcite grains.

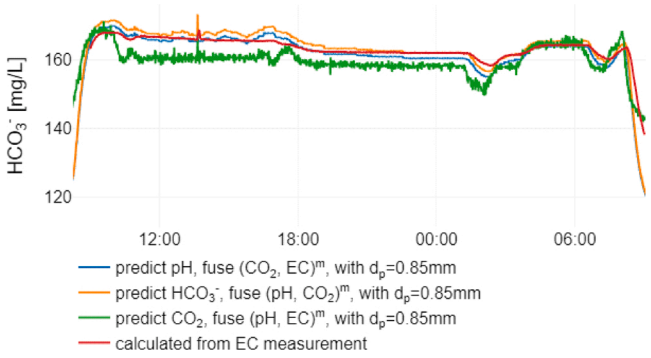

Fig. 12. Predicted bicarbonate concentration at the influent using different data fusion inputs from the influent (blue, orange, green line); the red line indicates bicarbonates concentration based on the measured EC of the effluent. The contactor is operated with a d_{50} of 0.85 mm calcite grains.

the data fusion predictions of another calcite filter run, but now the contactor has been filled with smaller grains ($d_{50} = 0.85$ mm) and the model parameter is set accordingly. The results of the different data approaches are similar to those observed with larger grains.

Finally, comparing Table 1 with Fig. 11 shows that the performance of the contactor is able to meet the requirements the aimed level of (calcium) hardness which is set at 1 mmol/L in the Dutch Drinking Water Directive [6]. Calcium (0.05 mg/L) and bicarbonate (9.9 mg/L) have very low concentrations at the inlet stream, hence, the increase of bicarbonate to a level of approximately 140 mg/L (for 1.5 mm grains) leads to a bicarbonate difference of 130 mg/L, i.e. 2.1 mmol/L. This would amount to a calcium level of 1.05 mmol/L, which meets the aimed hardness of drinking water within tolerance levels.

4. Conclusions

A pilot scale experiment showed the feasibility of predicting the bicarbonate and calcium content in the filtrate water of a calcite contactor by fusing the CO_2 and pH sensor data with a calcite dissolution model. In particular it is shown that:

- Monitoring the calcite content in mineralised reverse osmosis permeate water can be realised by a data fusion approach using CO_2 sensor data and either pH or electrical conductivity data. Using both CO_2 sensor data and either pH or EC measurements, yielded accurate predictions of Ca^{2+} or CO_2/bicarbonate concentrations in the filtrate

water. Accurate model calculations are not feasible with the combination of pH and EC measurements, because a small bias in either of these measurements lead to large errors in the modelled CO_2 equilibrium concentration, and consequently, large errors in the calculated calcite concentrations;

- Although the pH value of permeate water has high measurement uncertainty, sensitivity analysis and monitoring in a pilot scale set-up show that the calculations which are needed for determining the dissolution of calcite can be done reliably on the basis of CO_2 and pH under the assumption of a correctly calibrated CO_2 measurement device;
- Compiled literature values showed show a stronger dependency of dissolution rate on temperature compared to other operation conditions like grain size, superficial velocity or bed height;
- It is shown that the dissolution model can be applied successfully under low temperature (12 °C) conditions.

Declaration of Competing Interest

The authors report no declarations of interest.

Acknowledgements

The authors gratefully acknowledge Harmen van der Laan for the fruitful discussions on the obtained results and for his assistance during the set-up, operation and maintenance of the pilot scale equipment. The anonymous reviewers are thanked for their helpful feedback. Research activities have been financed by the drinking water supply company Oasen N.V. and co-financed by the premium scheme of the Top Sector Alliance for Knowledge and Innovation (TKI) of the Dutch Ministry of Economic Affairs.

Appendix A. Supplementary data

Supplementary material related to this article can be found, in the online version, at doi:https://doi.org/10.1016/j.jwpe.2021.102011.

References

[1] E. Gabbrielli, A tailored process for remineralization and potabilization of desalinated water, Desalination 39 (December) (1981) 503–520, https://doi.org/10/d7zzvb.
[2] L.N. Plummer, D.L. Parkhurst, T.M.L. Wigley, Critical Review of the Kinetics of Calcite Dissolution and Precipitation, ACS Publications, 1979.
[3] E.L. Sjöberg, Kinetics and Mechanism of Calcite Dissolution in Aqueous Solutions at Low Temperatures'. Stockholm, Sweden: Stockholm University, Faculty of Science, 1978. https://pubs.sub.su.se/65.pdf.
[4] J.W. Morse, R.S. Arvidson, The dissolution kinetics of major sedimentary carbonate minerals, Earth. Rev. 58 (1) (2002) 51–84, https://doi.org/10/fk5mqf.
[5] R.S. Arvidson, I.E. Ertan, J.E. Amonette, A. Luttge, Variation in calcite dissolution rates, Geochim. Cosmochim. Acta 67 (9) (2003) 1623–1634, https://doi.org/10/fwxb9m.
[6] Staatsblad van het Koninkrijk der Nederlanden, Dutch Drinking Water Directive (Drinkwaterbesluit)', 2011. https://wetten.overheid.nl/BWBR0030111/2018-07-01#BijlageA.
[7] H. Shemer, D. Hasson, R. Semiat, State-of-the-art review on post-treatment technologies, Desalination 356 (Supplement C) (2015) 285–293, https://doi.org/10.1016/j.desal.2014.09.035.
[8] M.D. Afonso, J.O. Jaber, M.S. Mohsen, Brackish groundwater treatment by reverse osmosis in Jordan, Desalination 164 (2) (2004) 157–171, https://doi.org/10.1016/S0011-9164(04)00175-4.
[9] M. Sarai Atab, A.J. Smallbone, A.P. Roskilly, An operational and economic study of a reverse osmosis desalination system for potable water and land irrigation, Desalination 397 (November) (2016) 174–184, https://doi.org/10.1016/j.desal.2016.06.020.
[10] M. Arora, R.C. Maheshwari, S.K. Jain, A. Gupta, Use of membrane technology for potable water production, Desalination 170 (2) (2004) 105–112, https://doi.org/10.1016/j.desal.2004.02.096.
[11] V. Albergamo, B. Blankert, E.R. Cornelissen, B. Hofs, W.-J. Knibbe, W. Van der Meer, P. de Voogt, Removal of polar organic micropollutants by pilot-scale reverse osmosis drinking water treatment, Water Res. 148 (January) (2019) 535–545, https://doi.org/10.1016/j.watres.2018.09.029.
[12] P.C. Kamp, J.C. Kruithof, H.C. Folmer, UF/RO treatment plant Heemskerk: from challenge to full scale application, Desalination 131 (1) (2000) 27–35, https://doi.org/10.1016/S0011-9164(00)90003-1.
[13] V. Albergamo, B.I. Escher, E.L. Schymanski, R. Helmus, M.L. Dingemans, E. R. Cornelissen, M.H.S. Kraak, J. Hollender, P. de Voogt, Evaluation of reverse osmosis drinking water treatment of riverbank filtrate using bioanalytical tools and non-target screening, Environ. Sci. Water Res. Technol. 6 (1) (2020) 103–116, https://doi.org/10.1039/C9EW00741E.
[14] R.D. Letterman, M. Hadad, C.T. Driscoll, Limestone contactors: steady-state design relationships, J. Environ. Eng. 117 (3) (1991) 339–358, https://doi.org/10.1061/(ASCE)0733-9372(1991)117:3(339).
[15] V. Yamauchi, K. Tanaka, K. Hattori, M. Kondo, N. Ukawa, Remineralization of desalinated water by limestone dissolution filter, Desalination 66 (1987) 365–383.
[16] D. Hasson, O. Bendrihem, Modeling remineralization of desalinated water by limestone dissolution, Desalination 190 (1–3) (2006) 189–200, https://doi.org/10/bh7vq3.
[17] H. Shemer, D. Hasson, R. Semiat, Design considerations of a packed calcite bed for hardening desalinated water, Ind. Eng. Chem. Res. 52 (31) (2013) 10549–10553, https://doi.org/10.1021/ie302975b.
[18] S. Ghanbari, Pilot Study and Modeling of Remineralization of Low-Temperature Desalinated Water by Calcite Filtration, Delft University of Technology, Delft, The Netherlands, 2018.
[19] H. Shemer, D. Hasson, R. Semiat, M. Priel, N. Nadav, A. Shulman, E. Gelman, Remineralization of desalinated water by limestone dissolution with carbon dioxide, Desalin. Water Treat. 51 (4–6) (2013) 877–881, https://doi.org/10/gdtj7g.
[20] D.L. Parkhurst, C.A.J. Appelo, Description of input and examples for PHREEQC version 3 a computer program for speciation, batch-reaction, one-dimensional transport, and Inverse geochemical calculations. US Geological Survey Techniques and Methods, Book 6, Modeling Techniques, 2013.
[21] O. Lehmann, L. Birnhack, O. Lahav, Design aspects of calcite-dissolution reactors applied for post treatment of desalinated water, Desalination 314 (2013) 1–9, https://doi.org/10.1016/j.desal.2012.12.017.